International Journal of Heat and Mass Transfer 53 (2010) 1575–1585

Contents lists available at ScienceDirect

International Journal of Heat and Mass Transfer

journal homepage: www.elsevier.com/locate/ijhmt

An investigation of a dual-reflection phenomenon of a natural convection in a three dimensional horizontal channel without Boussinesq assumption

Wu-Shung Fu [a,*], Chung-Gang Li [a], Ching-Chi Tseng [b]

[a] Department of Mechanical Engineering, National Chiao Tung University, Hsinchu 30056, Taiwan, ROC
[b] Department of Automation Engineering, Ta Hwa Institute of Technology, Dahua Road, Qionglin Shiang Hsinchu County 307, Taiwan, ROC

ARTICLE INFO

Article history:
Received 1 May 2009
Received in revised form 1 October 2009
Accepted 1 October 2009
Available online 7 January 2010

Keywords:
Dual-reflection
Natural convection
Boussinesq assumption
Horizontal channel
Reflection problems

ABSTRACT

An investigation of a dual-reflection phenomenon of a natural convection induced by a high temperature difference in a three dimensional horizontal channel is studied numerically. Because of a situation of high temperature difference, the Boussinesq assumption usually made in the natural convection problem is no longer available, the effects of the compressibility of fluid on all related factors must be considered. Solution methods of Roe, preconditioning and dual time stepping are appropriate for low speed compressible flow field and combined to solve the governing equations. For saving computation time, the computational process is parallel and 8 processors are used. At the aperture of the horizontal channel, the directions of fluid flows in the upper and lower regions are opposite which results in the reflection problems in the upper and lower regions induced by the large difference between the velocities of acoustic waves and fluids being completely different. The two different reflections phenomena occurring at the same aperture is conveniently named as a dual-reflection phenomenon which has never been investigated.

1. Introduction

Accompanying with minimization of devices, a superfluous space used to install a forced cooling system to remove useless heat energy is not admitted and the accumulation of useless heat energy generated by the devices becomes a main barrier to develop the device of higher level. Also, processes involving high temperature conditions in which a natural convection plays a role are continuously developed for many industrial applications such as a flow in a chimney, drying processes, solar receiver system, fire research and deposition processes in semiconductor manufacturing. As a result, a natural convection in an opened-ended finite length channel is still a very important subject in both academic and industrial researches. The coexistence of variable densities of fluids and slow velocities of flows is the characteristic of the above subject. For avoiding the complexity of the solving process caused by the characteristics mentioned above, the Boussinesq assumption in which a factor of the variable density of fluid only affects a buoyancy force is usually adopted when theoretical analyses of the natural convection are executed. As for the treatment of boundary conditions at the channel apertures, one of the methods of adjustment of the length for satisfying a fully developed flow [1–8], an adoption of effective boundary conditions at the aperture planes [9], and no pressure difference between the outlet and surroundings [6–8] is usually used. And the boundary condition at the inlet of the channel, a method of mass conservation or according to Bernoulli's equation is proposed [6–8].

According to Gray and Giorgini [10], when the temperature difference between the heat and cold sources of the natural convection problem is smaller than 30 K, the results obtained by the Boussinesq assumption are well consistent with the practical situation. However, in many other important natural convection problems mentioned earlier, the temperature differences are often higher than several hundred degrees. Because of the inapplicability of the Boussinesq assumption under the high temperature difference natural convection, the factor of compressibility of fluid which causes the problems to become very complicated should be then considered. Also, under a realistic condition the pressure difference between the inside and outside of the channel aperture is existent. Otherwise, the fluid from the outside could not flow into the channel and the fluid in the channel could not be discharged to the outside. This pressure difference would lead acoustic waves caused by the compressibility of fluid to reflect at the aperture [11]. And when the related numerical calculation is executed, the solutions in the channel are easily polluted by the reflections of the acoustic waves mentioned above which lead the computation processes to be poorly convergent, especially for a low speed compressible flow. Therefore, for analyzing the problem of natural convection in a channel under high temperature difference realistically, in addition to the consideration of the properties of viscosities and compressibility of fluid, the reflection problems at the aperture should also be considered simultaneously.

* Corresponding author. Address: Department of Mechanical Engineering, National Chiao Tung University, 1001 Ta Hsueh Road, Hsinchu 30056, Taiwan, ROC. Tel.: +886 3 5712121x55110; fax: +886 3 5720634.
E-mail address: wsfu@mail.nctu.edu.tw (W.-S. Fu).

0017-9310/$ - see front matter © 2009 Elsevier Ltd. All rights reserved.
doi:10.1016/j.ijheatmasstransfer.2009.11.019

Nomenclature

b	horizontal channel gap (m)
c	original acoustic wave speed (m/s)
c'	modified acoustic wave speed (m/s)
g	acceleration of gravity (m/s^2)
k	thermal conductivity (W/mK)
M	local Mach number
Nu	local Nusselt numbers defined in Eq. (27)
$\overline{Nu}$	average Nusselt number defined in Eq. (24)
$\widetilde{Nu}$	average Nusselt number defined in Eq. (29)
P	pressure (Pa)
P_0	surrounding pressure (Pa)
Pr	Prandtl number
$\dot{q}$	constant heat flux (W/m^2)
R	gas constant (J/kg/K)
Ra	Rayleigh number defined in Eq. (25)
Ra^*	Rayleigh number defined in Eq. (28)
$\widetilde{Ra}$	Rayleigh number defined in Eq. (30)
t	time (s)
T	temperature (K)
T_0	temperature of surroundings (K)
T_h	temperature of heat surface (K)
u, v, w	velocities in x-, y- and z-directions (m/s)
u'	Modified flow speed (m/s)
W	width of channel (m)
X	dimensionless Cartesian coordinates in x-direction
x, y, z	Cartesian coordinates (m)

Greek symbols

ρ	density (kg/m^3)
ρ_0	surrounding density (kg/m^3)
μ	viscosity (N s/m^2)
γ	specific heat ratio
θ	dimensionless temperature
β	thermal expansion coefficient (1/K)

For resolving the viscous compressible fluid in a low speed flow correctly, several related numerical methods had been proposed. In an explicit numerical method, the time step due to CFL (Courant-Friedrichs-Levy) condition is limited to an extremely small magnitude, and the convergent condition is difficult to be satisfied. In an implicit numerical method, the stiff situation causes an inefficiency of calculation to occur easily. For overcoming these defects mentioned above, Briley et al. [12] used a preconditioning method to improve the efficiency of calculation for a low Mach number flow, and adopted the implicit numerical method to resolve the convergent problem of the Navier-Stokes equation. Turkel [13] developed and applied a preconditioning matrix into problems of compressible and incompressible flows. Choi and Merkel [14] investigated convergent problems induced by the stiff situation and factorization error when an implicit numerical method was used to solve inviscid flow under a low Mach number flow. Moreover, the convergent problem of the Mach number of 0.05 flow was successfully resolved by using the precondition matrix. Afterward Choi and Merkel [15] proposed an adaptable preconditioning matrix to solve convergent problems of a viscous flow under a low Mach number situation. Roe [16] developed averaged variables method for compressible flow to solve discontinuous phenomenon occurring at a cell interface. This method has been widely used in solving compressible flow recently. Weiss and Smith [17] extended the researches of Choi, applied the Roe scheme mentioned above with preconditioning method into the solution method of three dimensional Navier-Stokes equations, and added a dual time stepping to resolve transient states of a low Mach number flow.

Also, in order to treat boundary conditions at the channel aperture of the compressible flow properly, Rudy and Strikwerda [18] proposed a concise non-reflecting boundary condition. Poinsot and Lele [11] developed the Navier-Stokes characteristics boundary condition (NSCBC) to resolve problems induced by boundary conditions of inlet, outlet and no slip on a wall. Polifke et al. [19] proposed a non-reflecting boundary condition modificated from NSCBC with the linear relaxation term and appear fully non-reflecting to plane acoustic waves with normal incidence on the boundaries for all frequencies. The velocities of flow fields investigated by both literatures mentioned above were larger than the Mach number of 0.3. Khanafer and Vafai [9] proposed a concise method to adopt effective boundary conditions obtained by a previous computation under an extended computational domain at the channel aperture. This method is for incompressible flows exclusively, and no reflection occurred at the channel aperture.

Relatively few researchers investigated natural convection problems in which the flow is regarded as a compressible fluid flow. Weiss and Smith [17] adopted the preconditioning method to simulate a natural convection in a two dimensional concentric circle. The temperatures of inner and outer walls were 2000 K and 1000 K, respectively. The corresponding Rayleigh number was about 4.7×10^4. The results showed that usage of the preconditioning method could reduce the computational time by approximately 60 times. Paillere et al. [20] used the preconditioning method to calculate a natural convection in a two dimensional enclosure. The results indicated that heat transfer rates obtained by the small temperature difference were close to these obtained by the Boussinesq assumption in spite of high temperatures of heat sources. All the studies mentioned above were in enclosure situations and did not consider the boundary conditions at the aperture. Yamamoto et al. [21] investigated a natural convection of a circular cylinder set in an external flow. The preconditioning method was used to calculate a compressible flow in a natural convection, and the results had good agreement with experimental results. Because of the external flow, the reflection problems induced by the reflection of acoustic waves at the aperture did not occur. As for a high temperature difference natural convection of a three dimensional horizontal channel which involves several complicated problems of a low speed compressible fluid flow, reflections of acoustic waves at apertures and unsuitability of the Boussinesq assumption is seldom investigated.

Therefore, the aim of this study is to investigate a subject of natural convection in a three dimensional horizontal channel numerically. In order to simulate the subject more realistically and broaden industrial applications, the channel is of an open-ended finite length and the temperature difference between the heat sources of the high and low temperatures is over several hundred degrees. The Boussinesq assumption is then no longer suitable for this study. A compressible fluid flow is taken into consideration instead of renunciation of the Boussinesq assumption. Since the influence of dimension factors on the natural convection in a horizontal channel is remarkable, and a model of three dimensional channel is used, solution methods of Roe, preconditioning and dual time stepping are combined to resolve the low compressible fluid flow in a transient state. Besides, a modification of the method proposed by Poinsot and Lele [11] is conducted to resolve the

reflection problems of velocity and temperature occurring at the apertures of the channel. For saving the computational time, the calculation process is parallel. The results show that at the aperture of the horizontal channel the directions of fluid flows in the upper and lower regions are opposite which results in the reflection problems in the upper and lower regions induced by the large difference between the velocities of acoustic waves and fluids being completely different. These two different reflections phenomena occurring at the same aperture are conveniently named as a dual-reflection phenomenon which has never been investigated yet. And the results of transient developments of pressure, flow and thermal fields are authenticated.

2. Physical model

A three dimensional horizontal channel which is open-ended and has finite length is regarded as a physical model and indicated in Fig. 1. The length, width and height are 11*W*, 2*W* and *W*, respectively. A heat surface of which the length and width are 2*W* and 2*W*, respectively, is installed on the center of the *xz*-plane. The temperature of the heat surface is T_h which is higher than the temperature T_0 of the surroundings. Except the heat surface region, the other regions are adiabatic. The gravity is downward and the temperature and pressure of the surroundings are 298.0592 K (T_0) and 101,300 Pa (P_0), respectively.

Since the temperature T_h of heat surface is higher, and a natural convection is produced in the channel. Ascending fluids caused the natural convection to impinge the top surface of the channel, and afterward the ascending fluids are divided into two parts which separately turn the flow directions to both apertures in the upper regions. In the meantime, cool fluids in the surroundings are sucked and via both of the apertures flow into the channel in the low regions to implement the ascending fluids. As a result, at the aperture the reflection problems caused by the large difference between the velocities of acoustic wave and fluid in the upper and lower regions are completely different. These two different reflections phenomena occur at the same interface are conveniently named as a dual-reflection phenomenon.

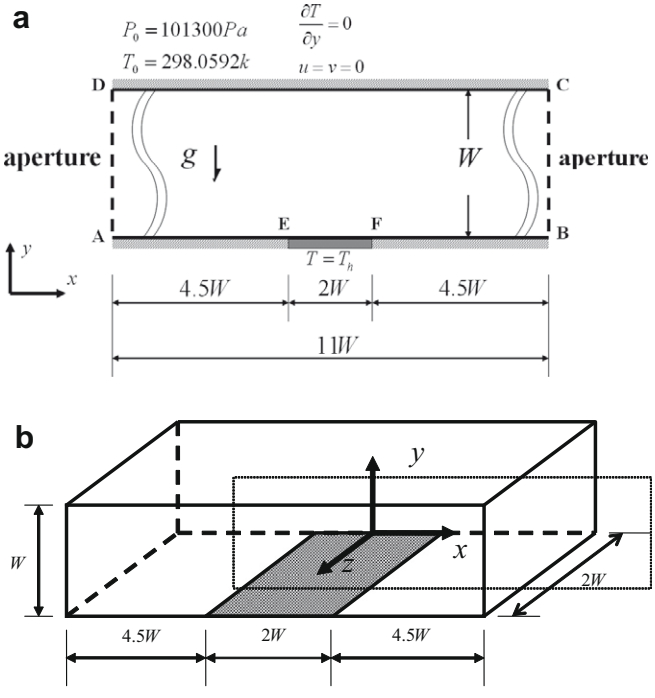

Fig. 1. Physical model.

For facilitating the analysis, the following assumptions are made.

1. The fluid is an ideal gas and follows the state of equation.
2. Fluid flows are laminar flows.
3. On the wall velocities satisfy no slip condition.
4. Except the heat surface, the other surfaces are adiabatic.

The governing equations in which the parameters of viscosity and compressibility of the fluid and gravity are considered simultaneously are shown in the following equations.

$$\frac{\partial U}{\partial t} + \frac{\partial F}{\partial x} + \frac{\partial G}{\partial y} + \frac{\partial \mathrm{H}}{\partial z} = S \tag{1}$$

$$P = \rho RT \tag{2}$$

The contents of *U*, *F*, *G*, *H* and *S* are indicated as follows.

$$\left.\begin{aligned} U &= \begin{pmatrix} \rho \\ \rho u \\ \rho v \\ \rho w \\ \rho E \end{pmatrix} \\ F &= \begin{pmatrix} \rho u \\ \rho u^2 + P - \tau_{xx} \\ \rho uv - \tau_{xy} \\ \rho uw - \tau_{xz} \\ \rho Eu + Pu - k\frac{\partial T}{\partial x} - u\tau_{xx} - v\tau_{xy} - w\tau_{xz} \end{pmatrix} \\ G &= \begin{pmatrix} \rho v \\ \rho u - \tau_{yx} \\ \rho v^2 + P - \tau_{yy} \\ \rho vw - \tau_{yz} \\ \rho Ev + Pv - k\frac{\partial T}{\partial y} - u\tau_{yx} - v\tau_{yy} - w\tau_{yz} \end{pmatrix} \\ H &= \begin{pmatrix} \rho w \\ \rho u - \tau_{zx} \\ \rho v - \tau_{zy} \\ \rho w^2 + P - \tau_{zz} \\ \rho Ew + Pw - k\frac{\partial T}{\partial z} - u\tau_{zx} - v\tau_{zy} - w\tau_{zz} \end{pmatrix} \\ S &= \begin{pmatrix} 0 \\ 0 \\ -(\rho - \rho_0)g \\ 0 \\ -(\rho - \rho_0)gv \end{pmatrix} \end{aligned}\right\} \tag{3}$$

The viscosity and thermal conductivity of the fluid are based upon Sutherland's law and shown as follows.

$$\left.\begin{aligned} \mu(T) &= \mu_0\left(\frac{T}{T_0}\right)^{\frac{2}{3}}\frac{T_0+110}{T+110} \\ k(T) &= \frac{\mu(T)\gamma R}{(\gamma-1)\mathrm{Pr}} \end{aligned}\right\} \tag{4}$$

where $\rho_0 = 1.1842\ \mathrm{kg/m^3}$, $g = 9.81\ \mathrm{m/s^2}$, $\mu_0 = 1.85 \times 10^{-5}\ N\,\mathrm{s/m^2}$, $T_0 = 298.0592$ K, $\gamma = 1.4$, $R = 287$ J/kg/K and Pr = 0.72.

3. Numerical method

In a natural convection, a speed of compressible fluid flow is much slower than that of an acoustic wave. The Roe method [16] coordinating preconditioning methods are then adopted to resolve

the governing equations shown in Eq. (1). To derive Eqs. (1) and (5) can be obtained.

$$\Gamma\frac{\partial U_p}{\partial\tau}+\frac{\partial F}{\partial x}+\frac{\partial G}{\partial y}+\frac{\partial H}{\partial z}=S \tag{5}$$

where Γ is a preconditioning matrix proposed by Weiss and Smith [17] and U_p is a primitive form of $[P, u, v, w, T]^t$.

In Eq. (5) a third order Runge-Kutta method which can be easily coded and paralleled is adopted to resolve the temporal term $\frac{\partial U_p}{\partial\tau}$.

Besides, the method of dual time stepping is added to calculate the transient state of the physical model. The derived equation is shown in Eq. (6).

$$\Gamma\frac{\partial U_p}{\partial\tau}+\frac{\partial U}{\partial t}+\frac{\partial F}{\partial x}+\frac{\partial G}{\partial y}+\frac{\partial H}{\partial z}=S \tag{6}$$

In the calculating processes of Eqs. (5) and (6), the contents of the term of F are divided into two parts of inviscid term $F_{inviscid}$ and viscous term $F_{viscous}$.

$$F_{inviscid=}\begin{pmatrix}\rho u\\ \rho u^2+P\\ \rho uv\\ \rho uw\\ \rho Eu+Pu\end{pmatrix} \tag{7}$$

$$F_{viscous}=\begin{pmatrix}0\\ -\tau_{xx}\\ -\tau_{xy}\\ -\tau_{xz}\\ -k\frac{\partial T}{\partial x}-u\tau_{xx}-v\tau_{xy}-w\tau_{xz}\end{pmatrix} \tag{8}$$

Utilize methods of the Roe [16] and preconditioning to calculate the magnitude of $F_{inviscid}$ at the position of $(i+\frac{1}{2})$ between the cells for low Mach number condition.

$$F_{inviscid,i+\frac{1}{2}}=\frac{1}{2}(F_R+F_L)-\frac{1}{2}\left\{|\Gamma^{-1}A_p|\Delta U_P\right\} \tag{9}$$

where $A_p=\left(\frac{\partial F}{\partial U_p}\right)$ is a flux jacobian.

A fourth order central difference is adopted to calculate $F_{inviscid}$

$$\frac{\partial u}{\partial x}=\frac{u_{i-2}-8u_{i-1}+8u_{i+1}-u_{i+2}}{12\Delta x}+o(\Delta x^4) \tag{10}$$

As for the boundary conditions at the apertures of the channel, in order to avoid the flow in the channel being polluted by the reflections of acoustic waves mentioned above, the non-reflecting boundary conditions are then necessarily used at the apertures of the channel.

In a high speed compressible flow condition, the method of LODI (local one dimensional inviscid relations) proposed by Poinsot and Lele [11] was suitably adopted for determining the non-reflecting boundary conditions at the apertures of the channel. However, a preconditioning matrix is not necessary in the above method that causes the method to be not appropriately adopted for determining the non-reflecting boundary conditions at the apertures of the channel under a low speed compressible flow. As a result, the modification of the method mentioned above is necessary for resolving the non-reflection boundary conditions under an extremely low speed compressible flow. The variations of densities of fluids are small near the regions of the apertures of the channel. The term of S indicated in Eq. (1) can be neglected. Then a flow field near the regions of the apertures of the channel can be approximately described by the following local one dimensional Navier-Stokes equation.

$$\Gamma\frac{\partial U_p}{\partial\tau}+\frac{\partial F}{\partial x}=0 \tag{11}$$

To multiply Γ^{-1} on the left side of Eq. (11), $\frac{\partial F}{\partial x}$ is transferred to be a primitive form.

$$\frac{\partial U_p}{\partial\tau}+\Gamma^{-1}\frac{\partial F}{\partial x}=0 \tag{12}$$

The term of $\Gamma^{-1}\frac{\partial F}{\partial x}$ can be expressed as the following form further.

$$\Gamma^{-1}\frac{\partial F}{\partial x}=\Gamma^{-1}\frac{\partial F}{\partial U_p}\frac{\partial U_p}{\partial x}=\Gamma^{-1}A_p\frac{\partial U_p}{\partial x} \tag{13}$$

Substitute Eq. (13) into Eq. (11), and obtain the following equation based on the primitive form.

$$\frac{\partial U_p}{\partial\tau}+\Gamma^{-1}A_p\frac{\partial U_p}{\partial x}=0 \tag{14}$$

A similar transformation of the term of $\Gamma^{-1}A_p$ is executed to obtain the characteristic velocities of the apertures of the channel.

$$\Gamma^{-1}A_p=K\lambda K^{-1} \tag{15}$$

where K is a eigenvector, λ are eigenvalues of the term of $\Gamma^{-1}A_p$, as well λ are characteristic velocities at the apertures of the channel. According to Dennis et al. [22], transform the orders of u (original flow speed) and c (original acoustic wave speed) into the similar orders of u' (modified flow speed) and c' (modified acoustic wave speed), and the following equation is obtained.

$$\lambda=\begin{pmatrix}\lambda_1\\ \lambda_2\\ \lambda_3\\ \lambda_4\\ \lambda_5\end{pmatrix}=\begin{pmatrix}u\\ u\\ u\\ u'+c'\\ u'-c'\end{pmatrix} \tag{16}$$

where $u'=\frac{(\Theta+1)u}{2}, c'=\frac{\sqrt{u^2(\Theta-1)^2+4\Theta c^2}}{2}$ and $\Theta\approx 100M^2$ according our test.Let

$$L=\lambda K^{-1}\frac{\partial U_p}{\partial x} \tag{17}$$

The contents of the term of L are

$$L=\begin{pmatrix}L_1\\ L_2\\ L_3\\ L_4\\ L_5\end{pmatrix}=\begin{pmatrix}u\frac{\partial T}{\partial x}+\frac{1}{\rho\gamma}\left(\frac{\partial P}{\partial x}-\gamma\frac{\partial P}{\partial x}\right)\\ u\frac{\partial w}{\partial x}\\ u\left(-\frac{\partial v}{\partial x}\right)\\ (u'+c')\left[\frac{\partial P}{\partial x}-\rho(u'-c'-u)\frac{\partial u}{\partial x}\right]\\ (u'-c')\left[\frac{\partial P}{\partial x}-\rho(u'+c'-u)\frac{\partial u}{\partial x}\right]\end{pmatrix} \tag{18}$$

The physical meaning of the term of L is the magnitude of wave amplitude with time variation.

Based on the characteristic velocities Eq. (16), the propagation speeds of L_1, L_2, L_3, L_4 and L_5 are u, u, u, $u'+c'$ and $u'-c'$, respectively. Substitute Eq. (17) into Eqs. (14) and (19) can be obtained.

$$\frac{\partial U_p}{\partial\tau}+KL=0 \tag{19}$$

Derive Eq. (19), the equations of pressure, velocities and temperature through the aperture of the channel are obtained, respectively.

$$\begin{aligned}&\frac{\partial p}{\partial\tau}+\frac{1}{2c'}[L_4(u'+c'-u)-L_5(u'-c'-u)]=0\\ &\frac{\partial u}{\partial\tau}+\frac{1}{2\rho c'}(L_4-L_5)=0\\ &\frac{\partial v}{\partial\tau}-L_3=0\\ &\frac{\partial w}{\partial\tau}+L_2=0\\ &\frac{\partial T}{\partial\tau}+L_1+\frac{1}{\rho}\frac{\gamma-1}{\gamma}\frac{1}{2c'}[L_4(u'+c'-u)-L_5(u'-c'-u)]=0\end{aligned} \tag{20}$$

The difference forms of Eq. (20) can be expressed as the following forms.

$$\begin{aligned} p^{k+1} &= p^k - \frac{\Delta\tau}{2\rho c'}[L_4(u'+c'-u) - L_5(u'-c'-u)] \\ u^{k+1} &= u^k - \frac{\Delta\tau}{2\rho c'}(L_4 - L_5) \\ v^{k+1} &= v^k + L_3\Delta\tau \\ w^{k+1} &= w^k - L_2\Delta\tau \\ T^{k+1} &= T^k - L_1\Delta\tau + \frac{1}{\rho}\frac{\gamma+1}{\gamma}(p^{k+1} - p^k) \end{aligned} \tag{21}$$

where k is an iteration number in artificial time.

Traditionally, when an investigation of natural convection in a vertical finite length channel is executed, a phenomenon of fluids from the inside of a channel via an aperture discharged to surroundings or fluids sucked from surroundings via an aperture flowing into a channel is usually encountered. Shown in Fig. 2(a), the magnitude of fluid velocity is larger than 0 and the direction of fluid velocity is from the inside of the channel to the surroundings. Under this situation, the directions of L_1, L_2, L_3, and L_4 are the same as that of the fluid velocity, and the magnitudes of L_1, L_2, L_3, and L_4 can be obtained from Eq. (18). Due to the negative magnitude of $(u' - c')$, the direction of L_5 is opposite to that of fluid velocity. The pressure at the infinite is invariant, the magnitude of $\frac{\partial p}{\partial \tau}$ is equal to 0 and the first equation of Eq. (20) becomes Eq. (22).

$$\frac{1}{2c'}[L_4(u'+c'-u) - L_5(u'-c'-u)] = 0 \tag{22}$$

Finally, the magnitude of L_5 can be obtained from Eq. (22)

$$L_5 = \frac{(u'+c'-u)}{(u'-c'-u)}L_4 \tag{23}$$

Oppositely, shown in Fig. 2(b) when the direction of fluid velocity is from the surroundings to the inside of the channel and the magnitude of fluid velocity is smaller than 0. The magnitude of L_4 can be obtained from Eq. (18) directly. Due to the existence of non-reflection condition at the aperture, the magnitudes of L_1, L_2, L_3 are set to be 0. The last one L_5 can be calculated from Eq. (23).

However, when a study of natural convection in a horizontal finite length channel is conducted. At the aperture, fluids flow streams from the inside of the channel to the surroundings are observed in the upper region, and fluids flow streams from the surroundings to the inside of the channel are observed in the lower region. These behaviors are indicated in Fig. 3 and named as a

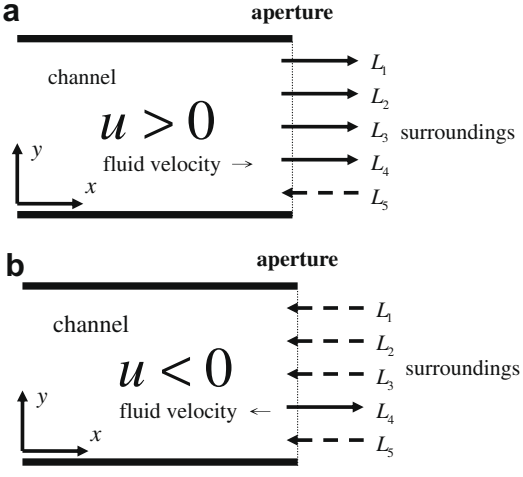

Fig. 2. The orientations of L_1, L_2, L_3, L_4 and L_5 at the aperture.

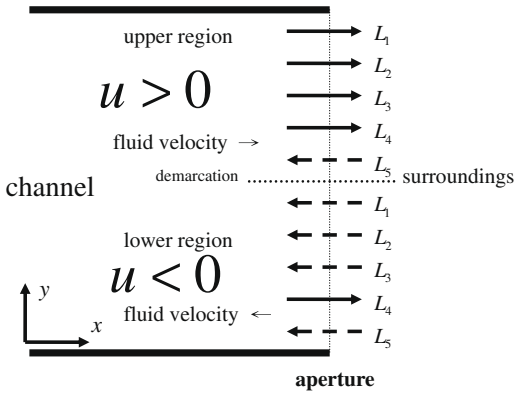

Fig. 3. A dual-reflection phenomenon at the aperture.

dual-reflection phenomenon. Usage of the methods mentioned above, in the upper region the magnitudes of L_1, L_2, L_3, and L_4 can be obtained from Eq. (18), and the magnitude of L_5 can be obtained from Eq. (23). In the lower region, because of non-reflection condition at the aperture the magnitudes of L_1, L_2 and L_3 are equal to 0. Since the magnitude of $(u' + c')$ is still larger than 0, the magnitude of L_4 is obtained from Eq. (18) and is the same as that in the upper region, subsequently the magnitude of L_5 can be obtained from Eq. (23). The region of demarcation which divides the channel into the upper and lower regions is composed of fluids having zero velocity.

A procedure calculating the equations mentioned above is briefly described as follows.

(1) Assign the initial conditions of the pressure, velocities and temperatures in the channel.
(2) Use Eqs. (18) and (21) to calculate the velocities, pressure and temperature at the aperture of the channel.
(3) Use MUSCL method to calculate Eq. (9), to obtain the magnitudes of F_R, F_L and ΔU_P .
(4) Substitute the magnitude of ΔU_P into Eq. (9) and use the Roe method to calculate the magnitudes of inviscid terms of $F_{inviscid}$.
(5) Calculate the magnitudes of viscous terms and substitute in Eq. (8).
(6) Use Runge-Kutta to obtain a new magnitude of U_p^{k+1} .
(7) Under a steady state, examine the convergence of the iterational computation of U_p^{k+1}. Repeat the processes from (2)–(6) until the convergent criteria are satisfied. The convergent criteria of variables are $\frac{\phi^{n+1}-\phi^n}{\phi^{n+1}} < 10^{-3}$, φ = p, u, v, w, T

Under a transient state, calculate Eq. (6) and examine the convergence of the iterational computation of the $\frac{\partial U_p}{\partial \tau}$. When the convergent condition is satisfied, the magnitude of U_p^{k+1} will be regarded as that of U_p of the $(n+1)th$ time step and the process proceeds to the next time step. In order to economize the consumption of computing time, parallel computations are executed by 8 processors.

4. Results and discussion

The working fluid is air and the Prandtl number is 0.72. Two grid distributions are used to examine the adoptable grid distribution. The results of distributions of u, v and T parallel to the y-axis at the position of $x = 5.5W$ and $z = W$ are shown in Fig. 4. The deviations of both the results obtained by the two grid distributions are slight, the uniform grid distribution of $220 \times 40 \times 40$ is used.

According to Gray and Giorgini [10], in a natural convection when the temperature difference of natural convection between

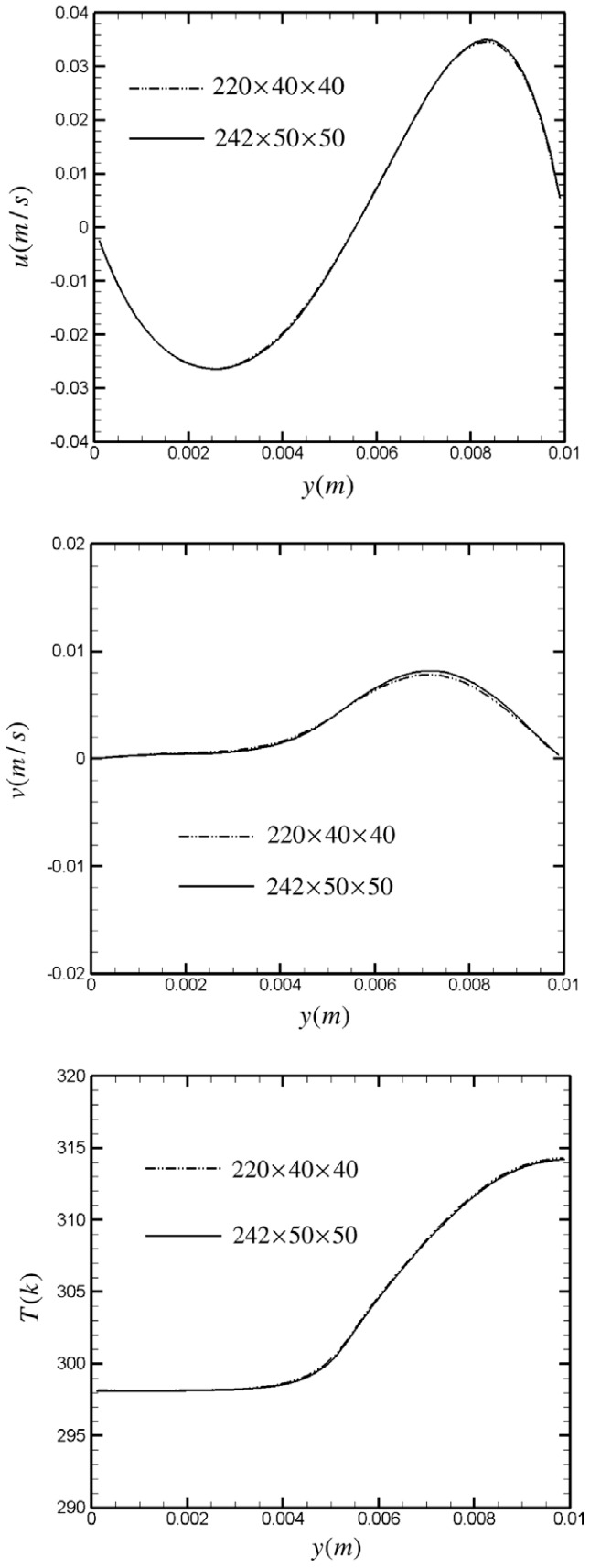

Fig. 4. Comparisons of velocities and temperature profiles along y-axis at the position of $x = 5.5W$, $z = W$ ($Ra^* = 10^4$).

two heat sources is smaller than 30 K, the results based on the Boussinesq assumption are well consistent with experimental results. In order to examine the suitability of this study under a low temperature difference, the temperature difference of two heat sources of 10 K is assigned and the computational method developed by this study in which the Boussinesq assumption is not yielded is used to investigate the same subject investigated by Davis [23], Khanafer and Vafai [9] and Andreozzi et al. [24]. The same physical models of Davis [23], Khanafer and Vafai [9] and Andreozzi et al. [24] are adopted, respectively. The definitions of average Nusselt number $\overline{Nu}$ and Rayleigh number Ra are shown as follows, respectively.

$$\overline{Nu} = \frac{1}{2W}\int \frac{W}{(T_h - T_c)}\left[\frac{\partial T}{\partial y}\right]_{wall} dx \tag{24}$$

$$Ra = \mathrm{Pr}\frac{g\rho_0^2\beta(T_h - T_c)W^3}{\mu^2} \tag{25}$$

where W is the height of the channel and β is the thermal expansion coefficient.

In Fig. 5, the isothermal lines of present results are compared with Davis [23]. The model of $Ra = 10^5$ is a cavity with the difference of temperature between the two vertical walls and adiabatic conditions in other two horizontal walls. The figures of isothermal lines of both results are almost completely consistent. Besides, the Nu_{max}, Nu_{min} and $\overline{Nu}$ of present results and Davis [23] are also tabulated in Table 1. The results of Nusselt numbers of both results also have good agreements. Base on the comparisons mentioned above, the accuracy of present method is positive.

The results shown in Fig. 6 are the comparisons of the distributions of streamlines and isotherms of the present study and Khanafer and Vafai [9]. The model used is a two dimensional channel, and the temperatures of upper and lower walls are constant, and the Rayleigh number is 10^4. The region indicated in the figure is a right half region. The boundary conditions on the aperture used in Khanafer and Vafai [9] were obtained from a previous computation with an extended boundary. The magnitudes of the gradient of variables assigned to be zero are the boundary conditions on the extended boundary when the previous computation with the extended boundary was executed. In this work, a non-reflection condition on the aperture is yielded, and the results in the channel can be resolved directly. Shown in the figures, in spite of the distribution of streamlines or isotherms, both the results have good agreements. Comparisons of the average Nusselt numbers of the present study and Khanafer and Vafai [9] are tabulated in Table 2. Due to the differences of numerical methods and properties of fluids between the present study and Khanafer and Vafai [9], the deviations of the magnitudes of average Nusselt numbers of the two studies mentioned above are difficult to exempt. In natural convection phenomena, the thermal situation on the lower heat wall is more unstable than that on the upper heat wall, and the acquirement of accurate average Nusselt number of the lower heat wall is more difficult than that of the upper heat wall. Then the deviations of the average Nusselt numbers of the lower side are usually larger than those of the upper side.

Shown in Fig. 7, comparisons of the distributions of upper and lower wall temperatures distributions of Andreozzi et al. [24] and present study are indicated. The nondimensional temperature is shown in the following equation.

$$\theta = \frac{(T - T_0)k}{\dot{q}b} \tag{26}$$

where $\dot{q}$ is a constant heat flux subject to the wall and b is the horizontal channel gap.

A constant heat flux $\dot{q}$ is separately added into the upper and lower walls of a two dimensional channel. For the same reason mentioned above, the deviations of the magnitudes of the

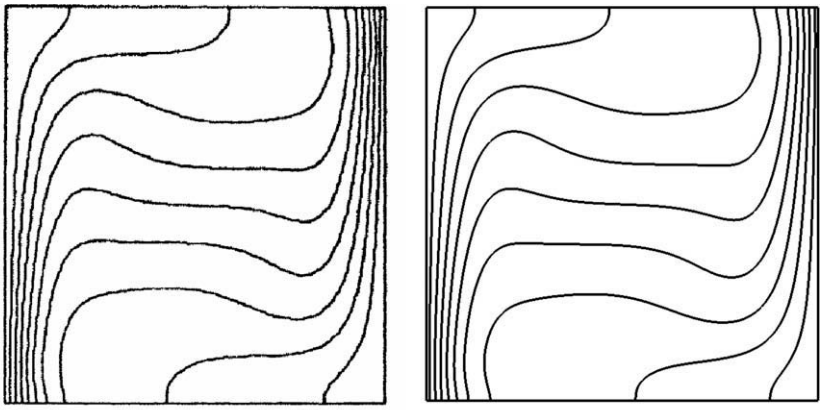

Fig. 5. Comparisons of isothermal line of the present results and results of Davis [23].

Table 1
Comparisons of the Nu_{max}, Nu_{min} and $\overline{Nu}$ of the present results and results of Davis [23].

	Results of Davis[23]	Present results	Error (%)
$\overline{Nu}$	4.519	4.509	0.22
Nu_{max}	7.717	7.698	0.25
Nu_{min}	0.729	0.751	3.02

temperatures between the two studies are existent. The maximum deviation is about 10%, and the variation trends are consistent.

In Fig. 8, the variations of thermal contour, steamlines, pressure contour and pressure differences with time are indicated for $Ra = 10^4$ situation. The plane is selected at the central position of the z-axis. The initial conditions of temperature and pressure in the channel are the same as those of the surroundings. As the heating process starts, the temperature of the heat surface is raised to 401.0490 K and kept at this temperature.

Shown in Fig. 8(1), $t = 0.0001$ s by means of a heat condition mode the temperatures of fluids above the heat surface rise first and the densities of these fluids become small. Thus the volume of these fluids is expanded and part of other fluids are pushed to flow out of the channel. This phenomenon is shown in Fig. 8(1b). The magnitude of the gray scale of pressure contour means the pressure differences between the pressures of fluids in the channel and the pressure of surroundings. The light fluids of which the densities are small form a thin dark region in which the pressures are relatively low shown in Fig. 8(1c). Due to the expansion of the light fluids, the original fluids above the dark region are suppressed which causes the pressures of original fluids to be raised and to push neighboring fluids to flow to the aperture. In the Fig. 8(1d), there are local pressure difference distributions of the four selected positions of 0, 1.8, 3.6 and 5.5 along y-axis to be indicated. The dashdotdot and solid lines mean the pressures of the surroundings and fluids at the selected local position, respectively. The intervals of the two lines indicate the pressure difference, and the scale of interval is in right proportion to the magnitude of pressure difference. The maximum magnitudes are annotated only. On the right side of the dashdotdot line means the pressures of fluids are larger than that of surroundings and vice versa. In this situation, all the pressures of fluids are larger than that of surroundings, then the fluids in the channel flow to the surroundings exclusively.

In Fig. 8(2), the time t is equal to 0.001 s. In Fig. 8(2a), a natural convection heat transfer starts to appear and affects the flow field which results in the isothermal lines in the left half region shown in the figure of thermal contour being distorted. Then a circulation zone is found in the left half region of the channel and indicated in Fig. 8(2b). The region near the heat surface in which the fluids absorb heat energy from the heat surface directly expands gradually and suppresses the above region that leads the pressure in the above region to be raised. This is shown in Fig. 8(2c). This behavior causes some fluids to be discharged to the surroundings. Due to the existence of circulation zone, the region in which the local pressure differences are negative appears in the lower portion of left half channel. In the right half channel, the fluids are still discharged to the surroundings, then the magnitudes of local pressure differences in this region are positive and shown in Fig. 8(2d).

Accompanying with the increment of time, the phenomena shown in Fig. 8(3) are similar to those shown in Fig. 8(2), and the influence of natural convection on the flow field almost expands to the whole region of the channel.

Shown in Fig. 8(4), the time t is equal to 0.01 s. The flow field caused by the natural convection is almost fully developed in the whole channel. In Fig. 8(4a), the variation of temperature distribution from the left to right sides of the channel is from the large to small magnitudes, and the isothermal lines are distorted which is a characteristic of convection phenomenon. Shown in Fig. 8(4b), a drainage which is composed of the fluids flowing into the channel from the surroundings in the low region of the aperture and vice versa in the upper region of the aperture in place of the circulation zone appearing in the figures mentioned above is observed. Above the heat surface, the lowest and highest pressure regions which mainly cause the fluid to flow into and out of the channel, respectively, are observed and shown in Fig. 8(4c). At the aperture of channel of Fig. 8(4d), the magnitudes of local pressure differences are positive and negative in the half upper and lower regions, respectively. This phenomenon occurring at the aperture is named as a dual-reflection phenomenon.

In Fig. 9, the distribution of isothermal surfaces at a steady state are indicated. The natural convection is fully developed in the channel that causes the isothermal surfaces to be distorted.

In Fig. 10, the distributions of local Nusselt numbers along z-direction at positions of $x = W$, and 0 are indicated, respectively. The local Nusselt number Nu and Rayleigh number Ra are defined as follows, respectively.

$$Nu = \frac{W}{k_0(T_h - T_c)}\left[k(T)\frac{\partial T}{\partial y}\right]_{wall} \tag{27}$$

$$Ra^* = \mathrm{Pr}\frac{g\rho_0^2(T_h - T_c)W^3}{T_0\mu(T)^2} \tag{28}$$

where W is the height of the channel.

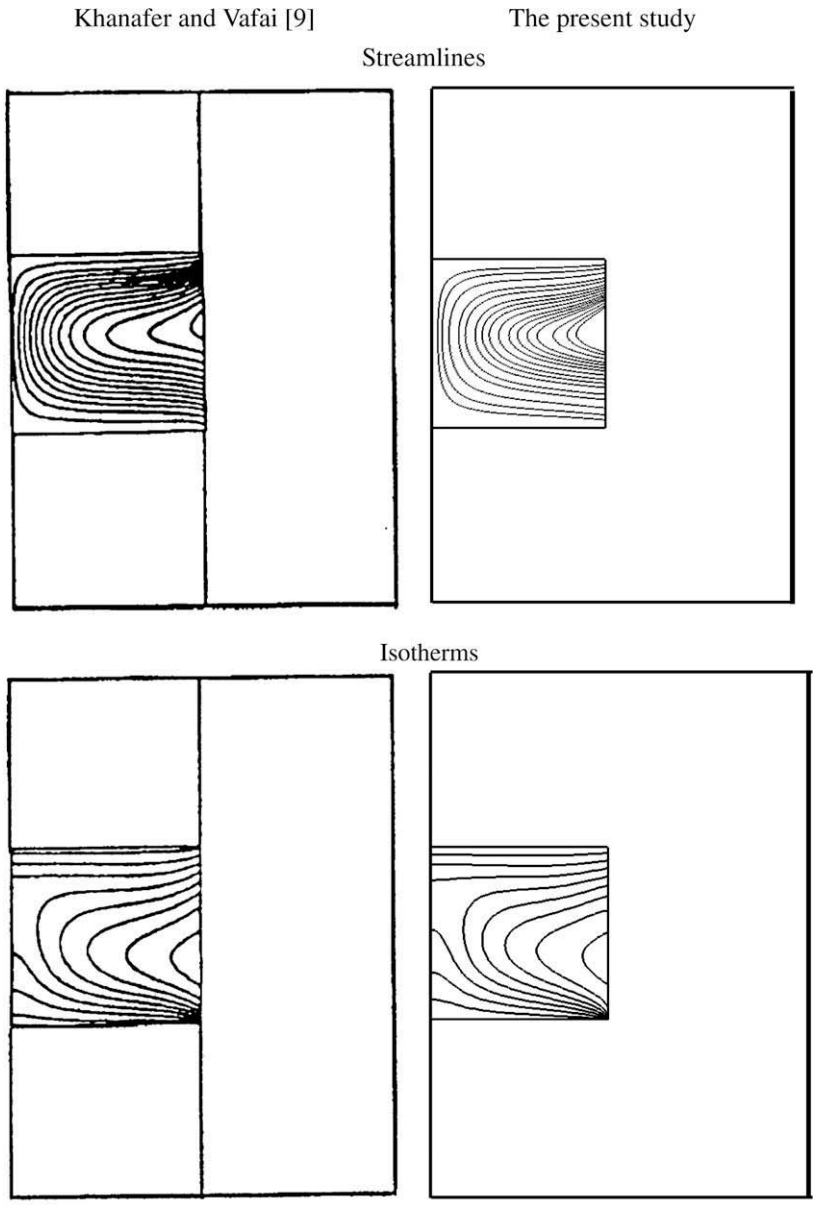

Fig. 6. Comparisons of the distributions of streamlines and isotherms of the present study and Khanafer and Vafai [9].

Table 2
Comparisons of the average Nusselt numbers of the present study and Khanafer and Vafai [9].

	Present study	Khanafer and Vafai [9]	Deviation (%)
$Ra = 10^4$			
Nu (lower)	2.20	1.99	10.0
Nu (upper)	1.10	1.09	0.5
	Present study	Khanafer and Vafai [9]	Percent dif. (%)
$Ra = 10^5$			
Nu (lower)	3.50	3.15	11.2
Nu (upper)	2.69	2.90	7.2

The position of center of the heat surface corresponds to $x = 0$, and the edge of the heat surface corresponds to $x = W$. Cool fluids contact with the heat surface at the position of $x = W$ first, thus the effect of heat transfer on the heat surface is the most apparent at this position, and the temperatures of cool fluids are then raised. Subsequently the heated fluids flow over the positions of $x = \frac{W}{2}$ and 0. The Nusselt numbers at the position of $x = \frac{W}{2}$ and 0 naturally decrease gradually. But the differences are slight between the positions of $x = \frac{W}{2}$ and 0. Due to the edge effect, Nusselt numbers on both sides are smaller than those at the center.

In Fig. 11, the distributions of local Nusselt numbers along x-direction at positions of $z = W$, $z = \frac{W}{2}$ and $z \cong 0$ are indicated, respectively. Because of the edge effect of side wall mentioned earlier, the distribution of local Nusselt numbers at the positions of $z \cong 0$ is smaller than those at the positions of $z = W$ and $\frac{W}{2}$, but the deviations among the three distributions are small.

Comparisons of the distributions of local Nusselt numbers on the central heat surface ($z = W$) for different Rayleigh numbers in which only the temperature differences are different are indicated in Fig. 12. The larger temperature difference naturally achieves the larger Nusselt number. However, the increasing rate of the Nusselt number is not proportional to that of temperature difference.

Average Nusselt number $\overline{Nu}^*$ and modified Rayleigh number $\widetilde{Ra}$ are defined as follows, respectively

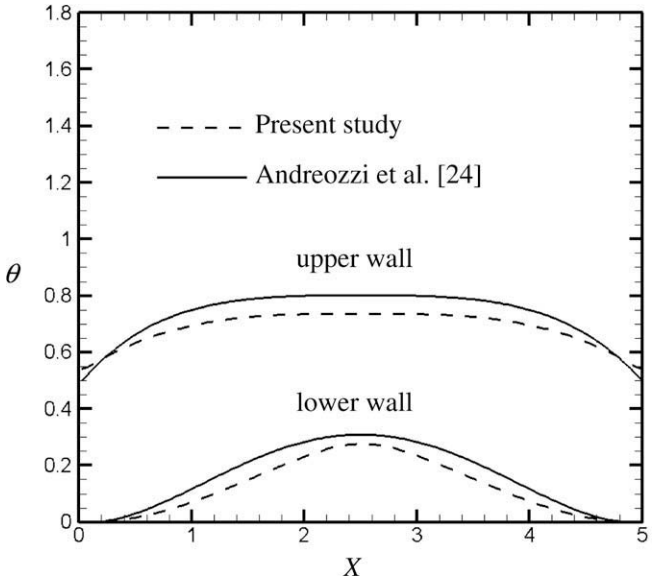

Fig. 7. Comparisons of the distributions of upper and lower wall temperatures at steady state.

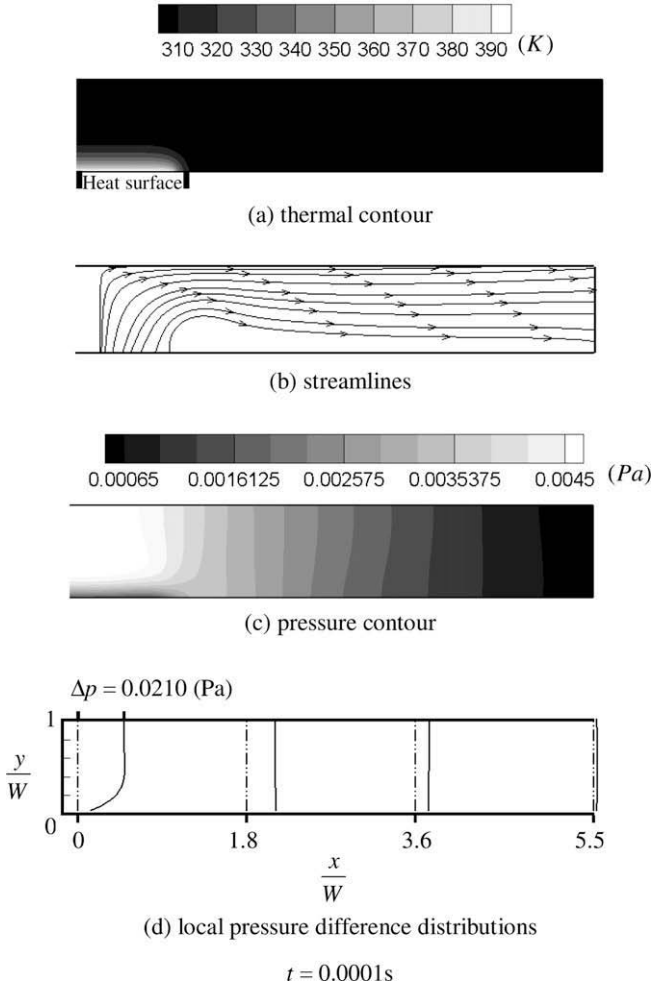

Fig. 8. (1) The variants of thermal contours, streamlines, pressure contour and pressure difference distributions with time under $Ra^* = 10^4$.

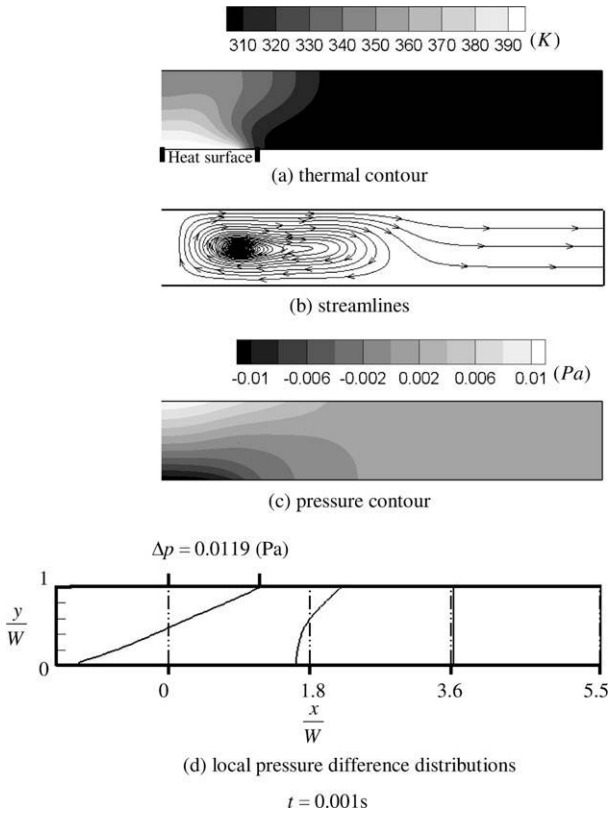

Fig. 8. (2) The variants of thermal contours, streamlines, pressure contour and pressure difference distributions with time under $Ra^* = 10^4$.

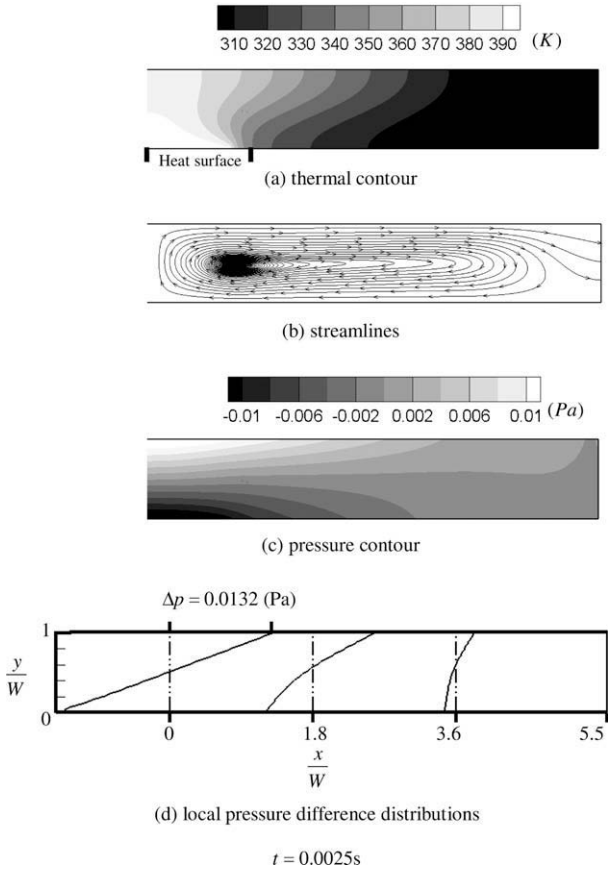

Fig. 8. (3) The variants of thermal contours, streamlines, pressure contour and pressure difference distributions with time under $Ra^* = 10^4$.

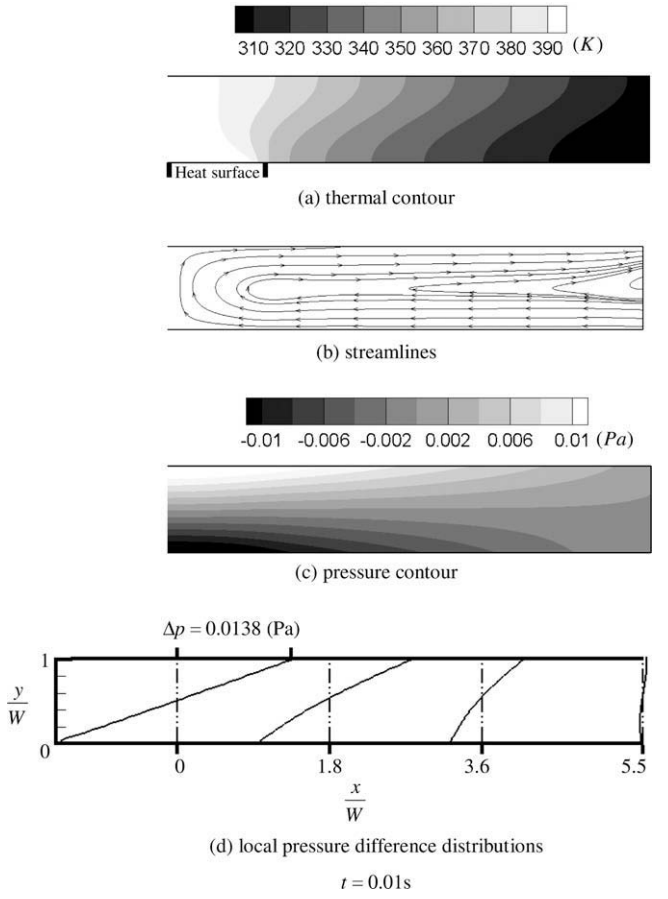

Fig. 8. (4) The variants of thermal contours, streamlines, pressure contour and pressure difference distributions with time under $Ra^* = 10^4$.

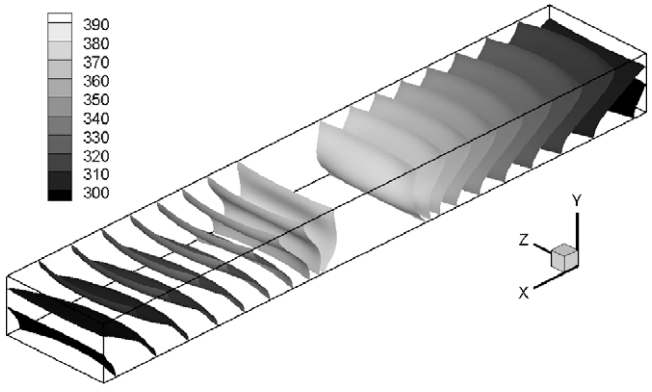

Fig. 9. The distribution of isothermal surfaces at a steady state.

$$\widetilde{Nu} = \frac{1}{A}\int\int \frac{(W/2)}{k_0(T_h - T_c)}\left[k(T)\frac{\partial T}{\partial y}\right]_{wall} dxdy \tag{29}$$

$$\widetilde{Ra} = \mathrm{Pr}\frac{g\rho_0^2(T_h - T_c)\times(W/2)^3}{T_0\mu(T)^2} \tag{30}$$

where A is the area of the heat surface and $W/2$ is the characteristic length of the heat surface according to Bejan [25].

The average Nusselt numbers obtained from this study can be expressed as a function of modified Rayleigh number and shown in the following equation.

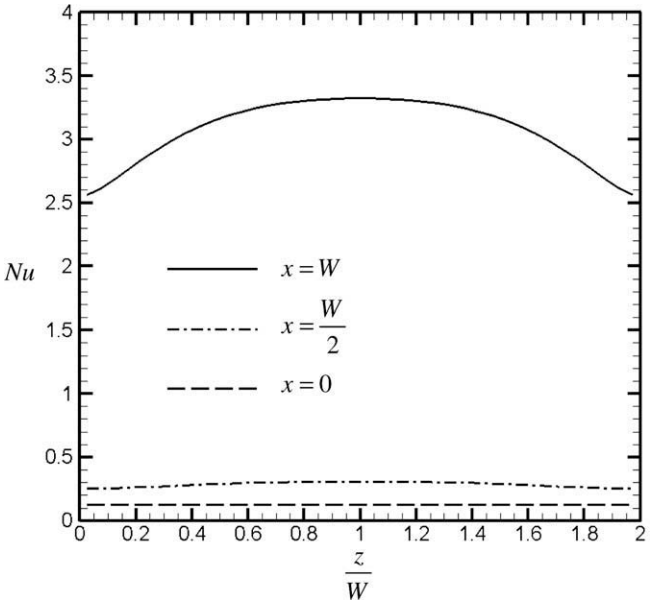

Fig. 10. The distributions of local Nusselt numbers along z-direction at positions of $x = W$, $x = \frac{W}{2}$ and $x = 0$.

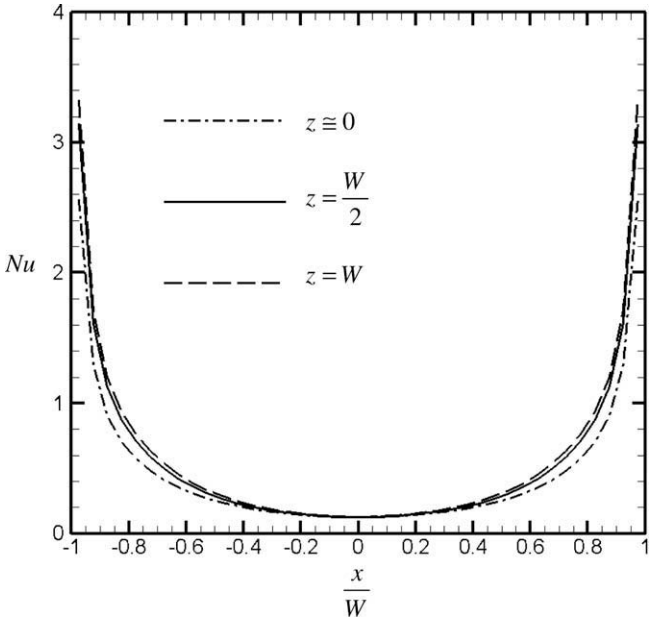

Fig. 11. The distributions of local Nusselt numbers along x-direction at positions of $z = W$, $z = \frac{W}{2}$ and $z \cong 0$.

$$\widetilde{Nu} = 0.019113 \times (\widetilde{Ra})^{0.3735} \tag{31}$$

The relationship between the average Nusselt number and modified Rayleigh number presents an exponential form. This trend is similar to those obtained by experimental works of Bejan [25] and Martorell et al. [26] for natural convection in an infinite space.

5. Conclusions

A natural convection induced by high temperature difference in a three dimensional horizontal channel is investigated without the Boussinesq assumption. Solution methods of the Roe scheme, preconditioning and dual time stepping are combined to resolve

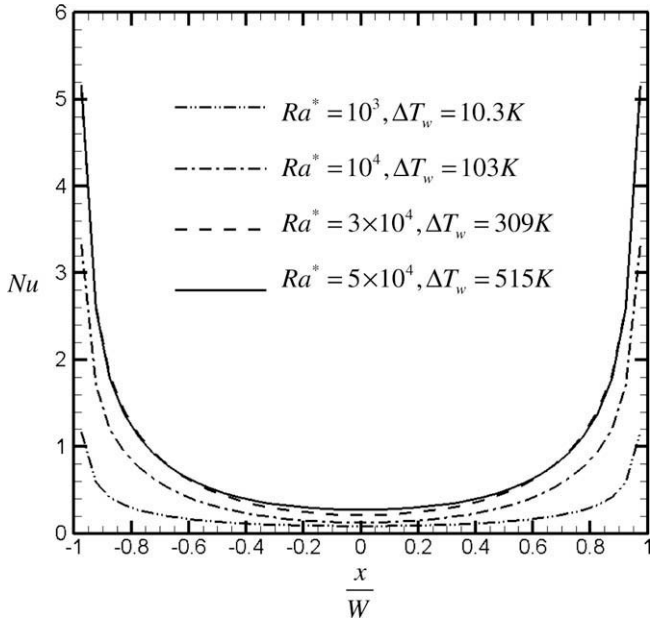

Fig. 12. Comparisons of the local Nusselt numbers on the heat surface for different Rayleigh numbers.

governing equations and non-reflecting conditions are adopted at the aperture. Several conclusions are summarized as follows.

1. Under a low temperature difference condition the results obtained by the Boussinesq assumption and this work are well consistent.
2. Under a high temperature difference condition in which the Boussinesq assumption is not held, the results obtained by this work are reasonable.
3. A dual-reflection phenomenon is observed at the aperture due to the opposite directions of fluid flows in the upper and lower regions of the aperture.
4. An average Nusselt number can be expressed as a function of the Rayleigh number in an exponential form.

Acknowledgement

The authors gratefully acknowledge the support of the Natural Science Council, Taiwan, ROC under Contact NSC96-2221-E-009-059, the Professor of Institute of Fluid Science, Tohoku University, Japan, Yasuaki KOHAMA, the support of Summer Program 2009 sponsored by Interchange of Association Japan and Natural Science Council, Taiwan, ROC and National Center for High-Performance Computing of Taiwan, ROC.

References

[1] P.H. Oosthuzien, A numerical study of laminar free convective flow through a vertical open partially heated plane duct, ASME HTD 32 (1984) 41–48.
[2] D. Naylor, J.M. Floryan, J.D. Tarasuk, A numerical study of developing free convection between vertical parallel plates, Trans. J. Heat Mass Transfer ASME 113 (1991) 620–626.
[3] D.A. Hall, G.C. Vliet, T.L. Bergman, Natural convection cooling of vertical rectangular channel in air considering radiation and wall conduction, J. Electron. Packag., Trans. ASME 121 (1999) 75–84.
[4] W.S. Fu, C.P. Huang, Effects of a vibrational heat surface on natural convection in a vertical channel flow, Int. J. Heat Mass Transfer 49 (2006) 1340–1349.
[5] J.M. Floryan, M. Novak, Free convection heat transfer in multiple vertical channels, Int. J. Heat Fluid Flow 16 (1995) 245–253.
[6] J.R. Dyer, The development of laminar natural-convective flow in a vertical uniform heat flux duct, Int. J. Heat Mass Transfer 18 (1975) 1455–1465.
[7] D. Gilles, F. Alberto, Laminar natural convection in a vertical isothermal channel with symmetric surface-mounted rectangular ribs, Int. J. Heat Mass Transfer 23 (2002) 519–529.
[8] S.A.M. Said, M.A. Habib, H.M. Badr, S. Anwar, Numerical investigation of natural convection inside an inclined parallel-walled channel, Int. J. Numer. Meth. Fluids 49 (2005) 569–582.
[9] K. Khanafer, K. Vafai, Effective boundary conditions for buoyancy-driven flows and heat transfer in fully open-ended two-dimensional enclosures, Int. J. Heat Mass Transfer 45 (2002) 2527–2538.
[10] D.D. Gray, A. Giorgini, The validity of the Boussinesq approximation for liquids and gases, Int. J. Heat Mass Transfer 19 (1976) 545–551.
[11] T.J. Poinsot, S.K. Lele, Boundary conditions for Navier-Stokes, J. Comput. Phys. 101 (1992) 104–129.
[12] W.R. Briley, H. McDonald, S.J. Shamroth, At low Mach number Euler formulation and application to time iterative LBI schemes, AIAA 21 (10) (1983) 1467–1469.
[13] E. Turkel, Preconditioned methods for solving the incompressible and low speed compressible equations, J. Comput. Phys. 72 (1987) 277–298.
[14] D. Choi, C.L. Merkel, Application of time-iterative schemes to incompressible flow, AIAA 25 (6) (1985) 1518–1524.
[15] D. Choi, C.L. Merkel, The application of preconditioning in viscous flows, J. Comput. Phys. 105 (1993) 207–223.
[16] P.L. Roe, Approximation Riemann solver, parameter vectors, and difference schemes, J. Comput. Phys. 43 (1981) 357–372.
[17] J.M. Weiss, W.A. Simth, Preconditioning applied to variable and constants density flows, AIAA 33 (1995) 2050–2056.
[18] D.H. Rudy, J.C. Strikwerda, A nonreflecting outflow boundary condition for subsonic Navier-Stokes calculations, J. Comput. Phys. 36 (1980) 55–70.
[19] W. Polifke, C. Wall, P. Moin, Partially reflecting and non-reflecting boundary conditions for simulation of compressible viscous flow, J. Comput. Phys. 202 (2005) 710–736.
[20] H. Paillere, C. Viozat, A. Kumbaro, I. Toumi, Comparison of low Mach number models for natural convection problems, Heat Mass Transfer 36 (2000) 567–573.
[21] S. Yamamoto, D. Niiyama, R.S. Beyong, A numerical method for natural convection and heat conduction around and in a horizontal circular pipe, Int. J. Heat Mass Transfer 47 (2004) 5781–5792.
[22] J. Dennis, P. Thomas, B. Pieter, Recent Enhancements to Overflow, Aerospace Sciences Meeting and Exhibit, 35th, Reno, NV, 1997.
[23] G.D.V. Davis, Natural convection of air in a square cavity a bench mark numerical solution, Int. J. Num. Meth. Fluids 3 (1983) 249–264.
[24] A. Andreozzi, Y. Jaluria, O. Manca, Numerical investigation of transient natural convection in a horizontal channel heated from the upper wall, Numer. Heat Transfer A 51 (2007) 815–842.
[25] A. Bejan, Convection Heat Transfer, John Wiley & Sons, Inc., 1995.
[26] I. Martorell, J. Herrero, F.X. Grau, Natural convection from narrow horizontal plates at moderate Rayleigh numbers, Int. J. Heat Mass Transfer 46 (2003) 2389–2402.